Enhanced performance of ZnO microballoon arrays for a triboelectric nanogenerator

2017 Nanotechnology 28 135401

(http://iopscience.iop.org/0957-4484/28/13/135401)

IOP Publishing Nanotechnology
Nanotechnology 28 (2017) 135401 (7pp) https://doi.org/10.1088/1361-6528/aa5f34

Enhanced performance of ZnO microballoon arrays for a triboelectric nanogenerator

Weili Deng[1], Binbin Zhang[1], Long Jin[1], Yueqi Chen[2], Wenjun Chu[2], Haitao Zhang[1], Minhao Zhu[1,3] and Weiqing Yang[1]

[1] Key Laboratory of Advanced Technologies of Materials (Ministry of Education), School of Materials Science and Engineering, Southwest Jiaotong University, Chengdu 610031, People's Republic of China
[2] School of Mechanical Engineering, Southwest Jiaotong University, Chengdu 610031, People's Republic of China
[3] State Key Laboratory of Traction Power, Southwest Jiaotong University, Chengdu 610031, People's Republic of China

E-mail: wqyang@swjtu.edu.cn

Received 8 September 2016, revised 21 November 2016
Accepted for publication 29 November 2016
Published 1 March 2017

Abstract

In recent years, triboelectric nanogenerators (TENGs), harvesting energy from the environment as a sustainable power source, have attracted great attention. Currently, many reports focus on the effect of surface modification on the electrical output performance of the TENG. In this work, we have fabricated vertically grown ZnO microballoon (ZnOMB) arrays on top of pyramid-featured PDMS patterned film, contacted with PTFE film to construct the TENG. The electrical output performances of the designed TENG are presented under external forces with different frequencies. The corresponding output open-circuit voltage with ZnOMBs could reach about 57 V the current density about 59 mA m^{-2} at 100 Hz, which was about 2.3 times higher than without any ZnO. The global maximum of the instantaneous peak power could reach 1.1 W m^{-2} when the external load resistance was about 2 MΩ. Furthermore, the electrical output of the fabricated device could light 30 commercial LED bulbs without any rectifier circuits or energy-storage elements. This clearly suggests that this kind of surface modification can dramatically enhance the output performance of the TENG. Moreover, the design of TENG demonstrated here can be applied to various energy harvesting applications.

Supplementary material for this article is available online

Keywords: ZnO microballoon arrays, triboelectric nanogenerator, PDMS, PTFE, pyramids

(Some figures may appear in colour only in the online journal)

1. Introduction

As we know, with rapid economic development and people's living standards constantly improving, the demand for energy is steadily on the increase. The energy crisis problem is becoming more and more prominent all over the world. Therefore, many scientists are trying to seek measures to avoid or alleviate the energy crisis. Among them, nanogenerators (NGs) [1, 2], harvesting natural environmental energy as a sustainable power source, have attracted great attention as a new kind of energy technology, including piezoelectronics [3–5], piezotronics [6, 7], and electrostatics [8–10]. In particular, the triboelectric nanogenerator (TENG) [11] has aroused much attention because of its high energy conversion efficiency [12–14], scalability [15–17], low cost [18–20], and fabrication simplicity [21–23], and this technology has been applied on various occasions [24–30]. After the first TENG was proposed in 2012 [8], many studies were carried out around enhancing the performance of the TENG, including material selection [31, 32], morphology optimization [33–35], structure design [36–38], theoretical guidance [39, 40], etc. The operating principle of the TENG for the case of dielectric-to-dielectric contact mode can be simply described by the coupling of contact charging and electrostatic induction

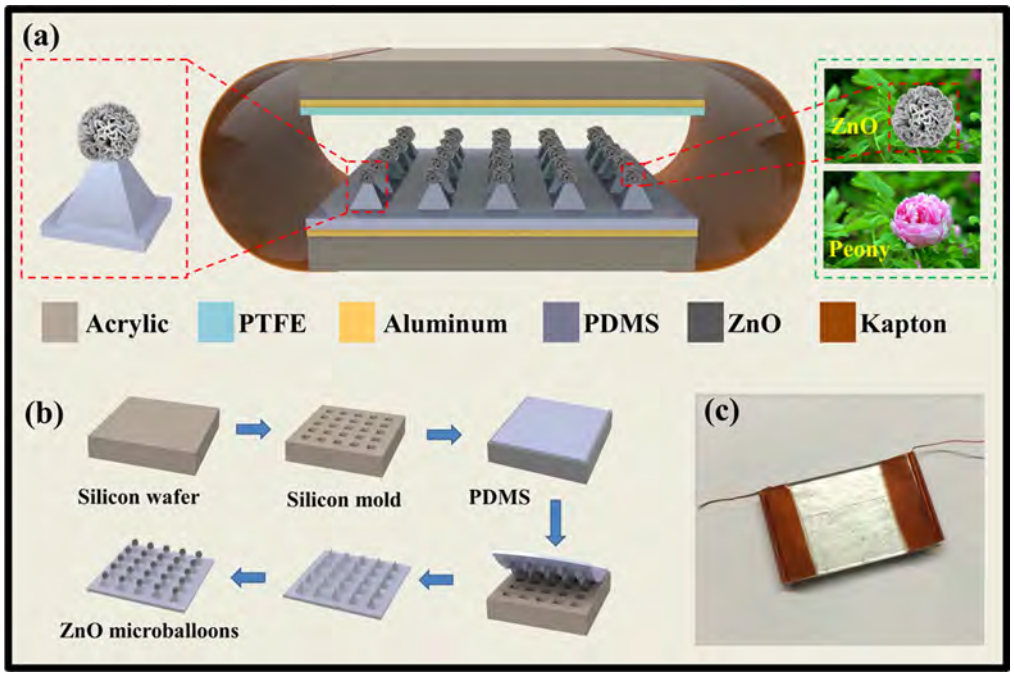

Figure 1. A schematic illustration of the PDMS-based TENG with ZnOMB arrays. (a) The fabricated TENG was composed of a sandwiched structure with two aluminum-foil-coated acrylic sheets, a layer of pyramid-patterned PDMS thin film with ZnOMB arrays and a layer of PTFE film. An enlarged view of the pyramid and ZnOMBs is shown in the top left corner. A comparison of a ZnOMB and a peony is in the top right corner. (b) The silicon wafer was patterned through photolithography, and served as the mold for fabrication of the PDMS thin film with pyramid pattern after wet etching. Then the ZnOMB arrays were synthesized on top of the pyramid structure through the hydrothermal method. (c) A photographic image of the fabricated TENG.

[41]. A typical TENG structure was a sandwiched structure with two different dielectric sheets stacked alternatively without interlayer binding [8]. Thus, the surface morphology and interface between the dielectric materials and electrodes are very important for the performance of the TENG.

In order to investigate the effect of surface microstructures on the electrical performance of the TENG, the Zhonglin Wang group has made a detailed comparative characterization of the devices with different PDMS (polydimethylsiloxane) features, clearly revealing that the output efficiency of TENGs with different surface microstructures should follow the order film < line < cube < pyramid [42]. Hence, we directly chose the pyramid-featured PDMS film for the further research on the effect of the surface morphology. In this work, we fabricated a novel structured TENG based on PDMS film which was decorated with ZnO microballoons (ZnOMBs) mounted on top of the pyramids. In the demonstration, the ZnOMBs have vertically grown out of the top point of every uniform pyramid on the PDMS film, and look like blooming flowers. These ZnOMBs were synthesized through a simple, low-cost, low-temperature hydrothermal method, which can facilitate large-scale production and preparation. The electrical output of a TENG with surface modification of ZnOMBs could reach 57 V at 100 Hz, about 2.3 times higher than that without any ZnO materials. This clearly suggests that this kind of surface modification can dramatically enhance the electrical output of the TENG, providing a unique microstructured material for the TENG.

2. Experimental details

The brief fabrication process and the final device structure of the PDMS-based TENG with ZnOMB arrays are shown in figure 1.

The fabricated TENG consisted of two dielectric layers, top and bottom electrodes and shells. Both the electrodes were made of aluminum foil, and were each fixed on acrylic sheets. One of the dielectric layers was PTFE (polytetrafluoroethylene); the other one was PDMS film decorated with pyramid patterns and ZnOMBs. To obtain pyramid-featured PDMS film, silicon molds were fabricated through photolithography and wet etching. A Si wafer, 3 in. (100), coated with silicon dioxide layers of about 300 nm, was patterned using photolithography, and then the patterned wafer was etched using BOE (buffered oxide etchant) solution. After washing off the photoresist with acetone and ethanol, the patterned wafer was etched anisotropically by wet etching with 6% potassium hydroxide solution at 90 °C, resulting in the formation of recessed pyramids as illustrated in figure 1. After being cleaned with acetone and isopropanol, all of the Si masters were treated with trimethylchlorosilane by gas phase silanization to avoid adhesion between the PDMS and Si molds [42]. In preparing the patterned films, PDMS elastomer and cross-linker were mixed in a 3:1 ratio (w/w), degassed and then coated on the Si masters. After incubation at 45 °C for 8 h, a uniform PDMS thin film was peeled off from the Si mold and then a copper layer of about 300 nm and a ZnO film of about 100 nm were successively deposited on

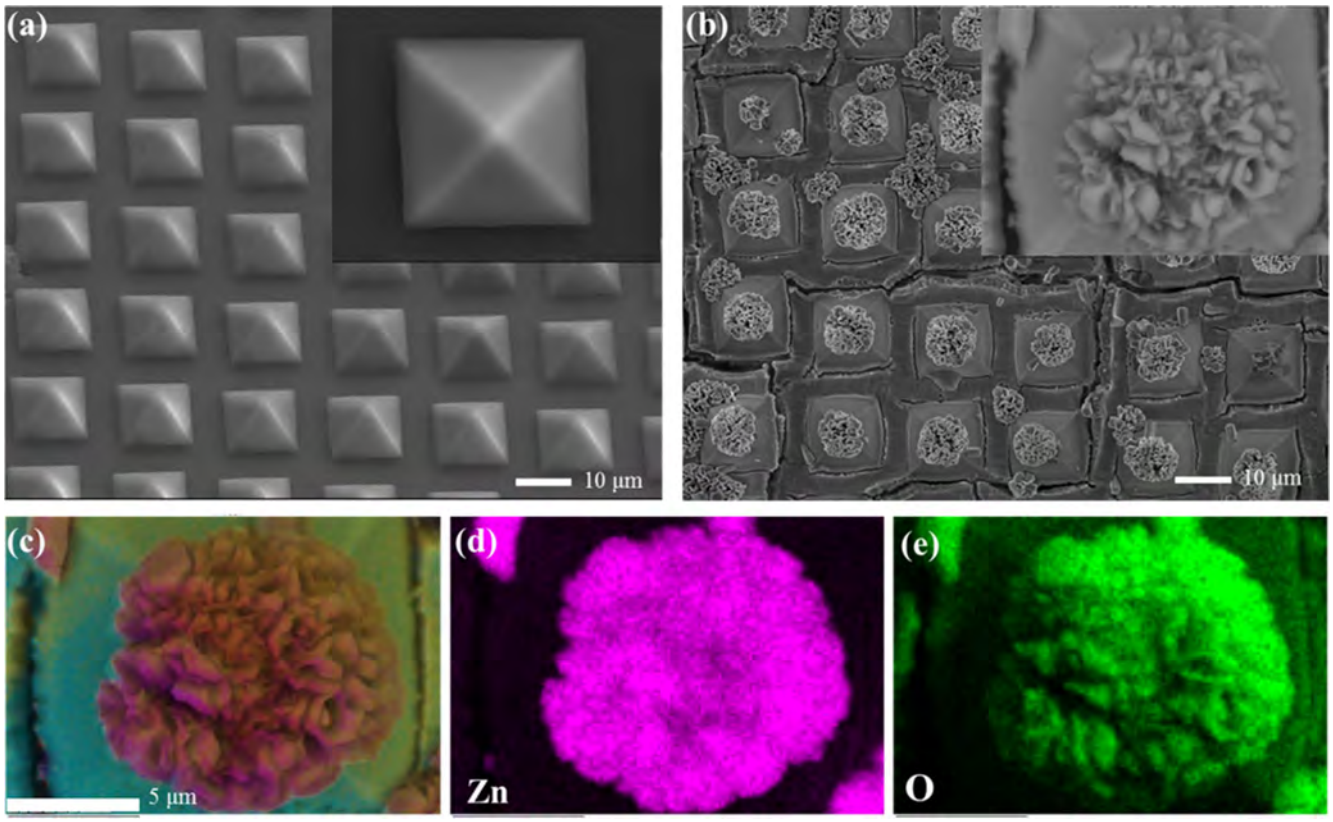

Figure 2. Structure characterization of the patterned PDMS thin film and the film with ZnOMBs. (a) SEM image of the patterned PDMS thin film with pyramid patterns. The inset is a vertical-view high-magnification image showing the pyramid structure of the features. (b) SEM image of the pyramid-patterned PDMS film with ZnOMBs. The inset is a vertical-view high-magnification image showing the ZnOMB features on the pyramid structure. Elemental color mapping of PDMS film with pyramid patterns and ZnOMBs: (c) the total color mapping of all the elements, (d) the elemental color mapping of zinc, and (e) the elemental color mapping of oxygen.

the fabricated PDMS film through the evaporation technique. The copper layer served as a buffer layer and the ZnO film as a seed layer. Then, the ZnO-seed-coated PDMS film was immersed into a nutrient solution to grow ZnO via a low-temperature hydrothermal method. The nutrient solution we used in the chemical growth process was an aqueous solution of $Zn(NO_3)_2 \cdot 6H_2O$ and HMTA (hexamethylenetetramine), and the concentration was 0.1 M [43]; the process was carried out in a convection oven at 85 °C for 12 h. At the end of the reaction, the PDMS film was taken out of the solution, rinsed with DI (deionized) water, and then dried. By this time, ZnOMBs have been synthesized on the pyramid pattern of PDMS film. After this, the PDMS film was placed on a piece of acrylic with the ZnO layer upwards. Finally, another clean acrylic-sheet-coated aluminum foil and PTFE film was placed onto the prepared PDMS substrate to form a sandwiched structure. Finally, both the short sides of the acrylic sheets were fixed with Kapton tape [44], whose role was to provide the restoring force to separate the acrylic sheets when they contacted with each other after the external force was removed. The photographic image of the fabricated TENG is shown in figure 1(c); its size was 3 cm × 2 cm, and the distance between the two electrodes, controlled by Kapton tape, was about 3 mm when they were completely separated.

3. Results and discussion

Like many other reports about TENGs [41, 42, 45], we have also fabricated some patterns on the polymer surfaces to enhance the triboelectric power output. However, the most distinctive part of this work is that we have directly synthesized many ZnOMBs on the pyramid structures, which look like flowers blooming on mountains. As shown in figure 1(a), an enlarged view of the ZnOMB-decorated pyramid is shown in the red box, compared with a peony in the green box, which looks very similar. (The detailed steps and parameters have been described in the 'Experimental details' section).

The morphology of ZnOMBs mounted on top of PDMS pyramids were further observed by employing scanning electron microscope technology. In figure 2(a), it can be observed that the pyramid pattern is regular and uniform across the whole area; the shape and lateral dimensions of the polymer structure are well controlled by the initial patterns on the surface of the wafer mold. From the magnified view of the SEM image in the inset, the pyramid is very angular and the lengths of the edges are homogeneous. As shown in figure 2(b), the as-prepared ZnO is well defined flower-like 3D microstructures with diameters in the range of 5–7 μm, which are assembled by many nanosheets as 'petals'. In addition, from the enlarged view of the SEM image in the

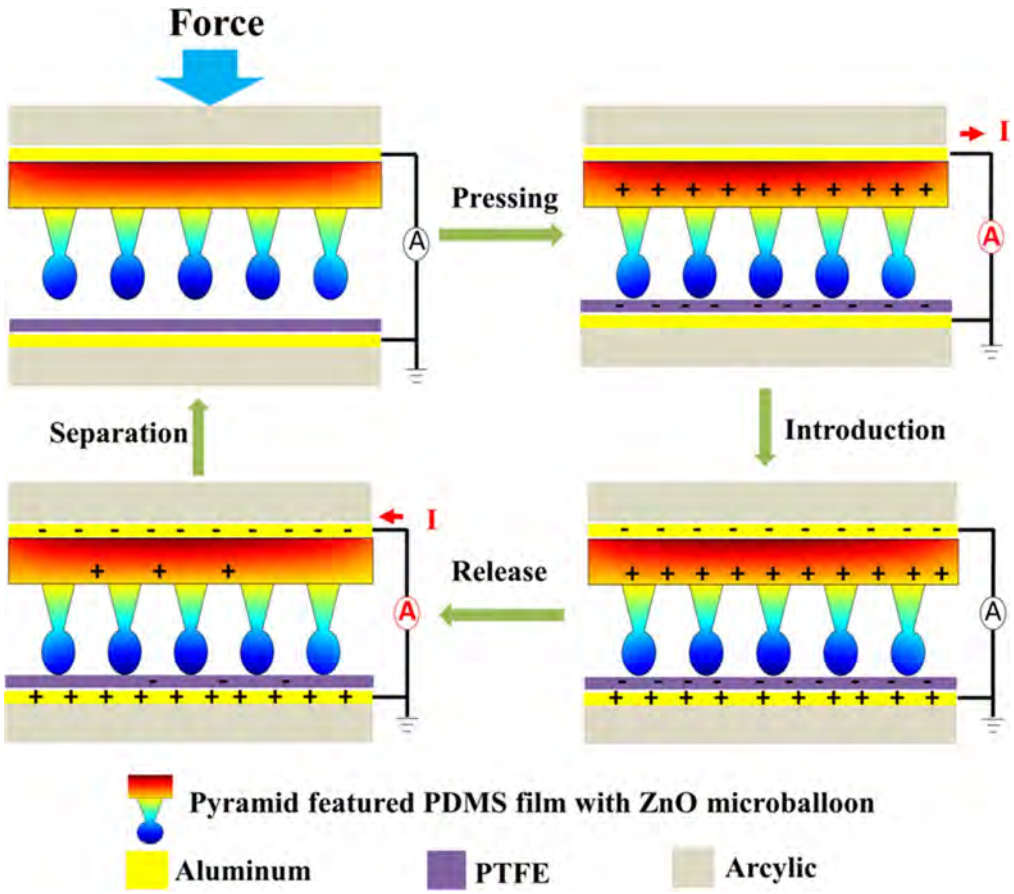

Figure 3. Working mechanism of the sandwich-shape TENG. Schematic illustration of the charge-generating process of the TENG. Pushed by the external force from the linear motor, the device will be switching back and forth between the separated state and the contacted state, and there will be an alternating flow of electrons in the external circuit driven by the induced triboelectric potential. The electric charges move for neutralization after the separation, forming a cycle.

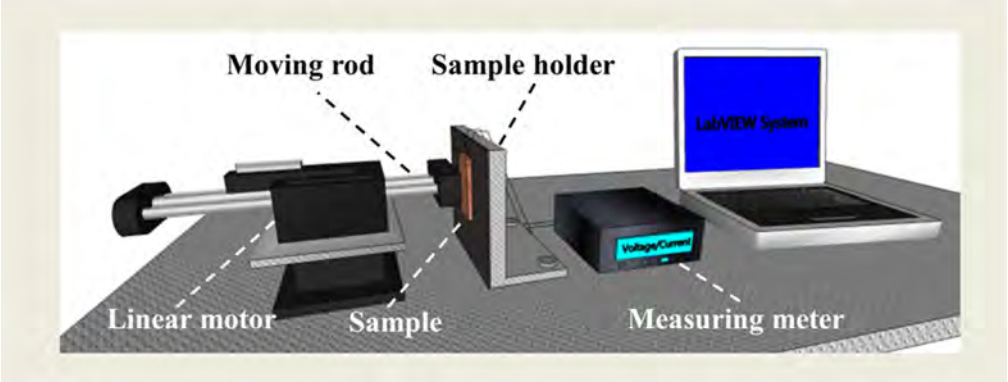

Figure 4. Schematic illustration of the measuring system for the typical electric output of the fabricated TENG.

inset, these nanosheets are not aggregated, in spite of their quite small size and ultrathin layers, and more importantly the ZnOMBs grow vertically on top of every pyramid. This structure can greatly enhance the effective contact area of the TENG when the opposite dielectric layer is pressed on the ZnOMBs, because the ZnOMBs protrude from the PDMS film surface, and the spheres have 3D hierarchical nanostructure, which is advantageous to contact with the non-flat part of the opposite layer. Hence, this structure has better friction performance, and it is more suitable for triboelectric devices. Furthermore, energy dispersive spectrometer (EDS) mapping is performed to investigate the contents of the ZnOMBs. From figures 2(c)–(e), it is easy to see that the zinc and oxygen elements are well distributed in the ZnOMBs.

Theoretically, for the working principle of the TENG, a schematic illustration is shown in figure 3. Under the external pressing force, the two acrylic sheets contact with each other, and charges are transferred due to the triboelectric effect.

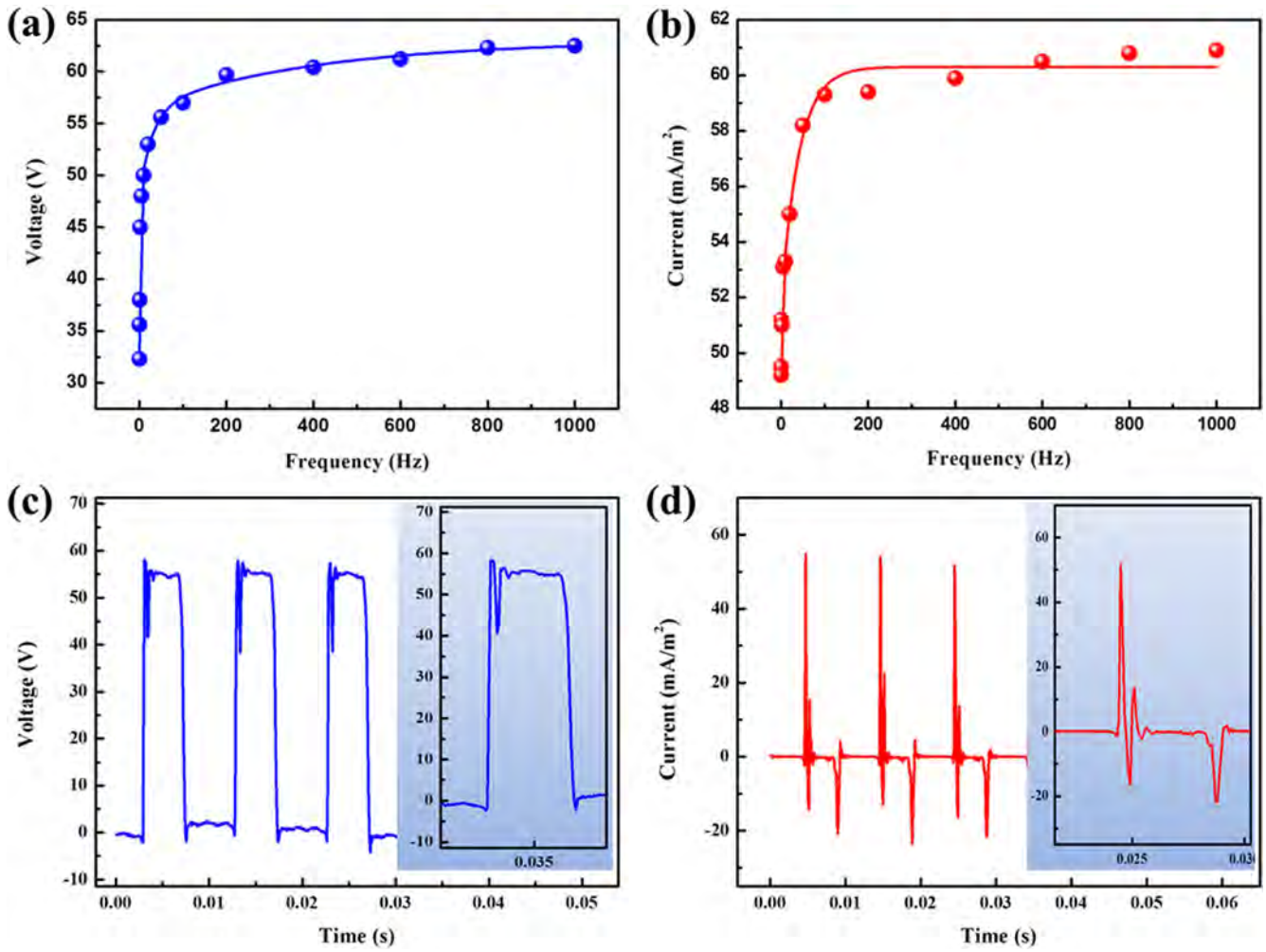

Figure 5. The typical electrical characteristics of the fabricated TENG. (a) Open-circuit voltage as a function of the motor's frequency. The curve is a fitted result. (b) Short-circuit current density as a function of the motor's frequency. The curve is a fitted result. (c) Open-circuit voltage at a push frequency of 100 Hz. Inset: enlarged view of one cycle. Separation causes the voltage to rise to a peak value and contact makes it fall back to zero. (d) Short-circuit current density at a triggering frequency of 100 Hz. Inset: enlarged view of one cycle. Contact and separation correspond to a positive current pulse and a negative current pulse, respectively, presenting an alternating-current (AC) characteristic.

When the two acrylic sheets are separated and contacted, under the driving of the electrostatic induction, a change in system capacitance drives the to-and-fro flow of the free electrons across the electrodes and leads to the flow of current in the external load [8]. In the designed structure, on the one hand, the emergence of ZnOMBs enlarge the interfacial region of the dielectric layer, which leads to a larger equivalent capacitance for the TENG. On the other hand, due to the piezoelectric effect of ZnO, the movement of charges will be enhanced. As a result, both the larger equivalent capacitance and the coupling between the piezoelectric and triboelectric outputs can achieve better electrical performance [46].

In order to measure output voltage and current characteristics of the fabricated TENG, different kinds of external mechanical force were applied on the TENG through a programmable linear motor. A schematic diagram of the measuring system is given in figure 4. In this setup, one end of the TENG was tightly fixed on the sample holder while the other end was dangling in the air; both the TENG and the driven rod of the linear motor were fixed in the same horizontal plane to ensure the driven rod could aim at the center of the TENG. During the measurement, the linear motor was programmed to push/pull the lateral rod with a specified distance, acceleration, maximum speed and deceleration, so that the TENG was pressed and released in a well controlled manner. The outputs of the TENG were detected by different measuring meters, and the data could be displayed and saved through a computer with the LabVIEW system.

To systematically investigate the performance of the TENG, a series of triggering frequencies were loaded on the driven rod. Figures 5(a) and (b) present the open-circuit voltage V_{oc} and short-circuit current I_{sc} density as a function of the motor's frequency from 0.2 Hz to 1000 Hz. Both the V_{oc} and I_{sc} of theTENG increase with the triggering frequency, and reach maximum values of 62.4 V and

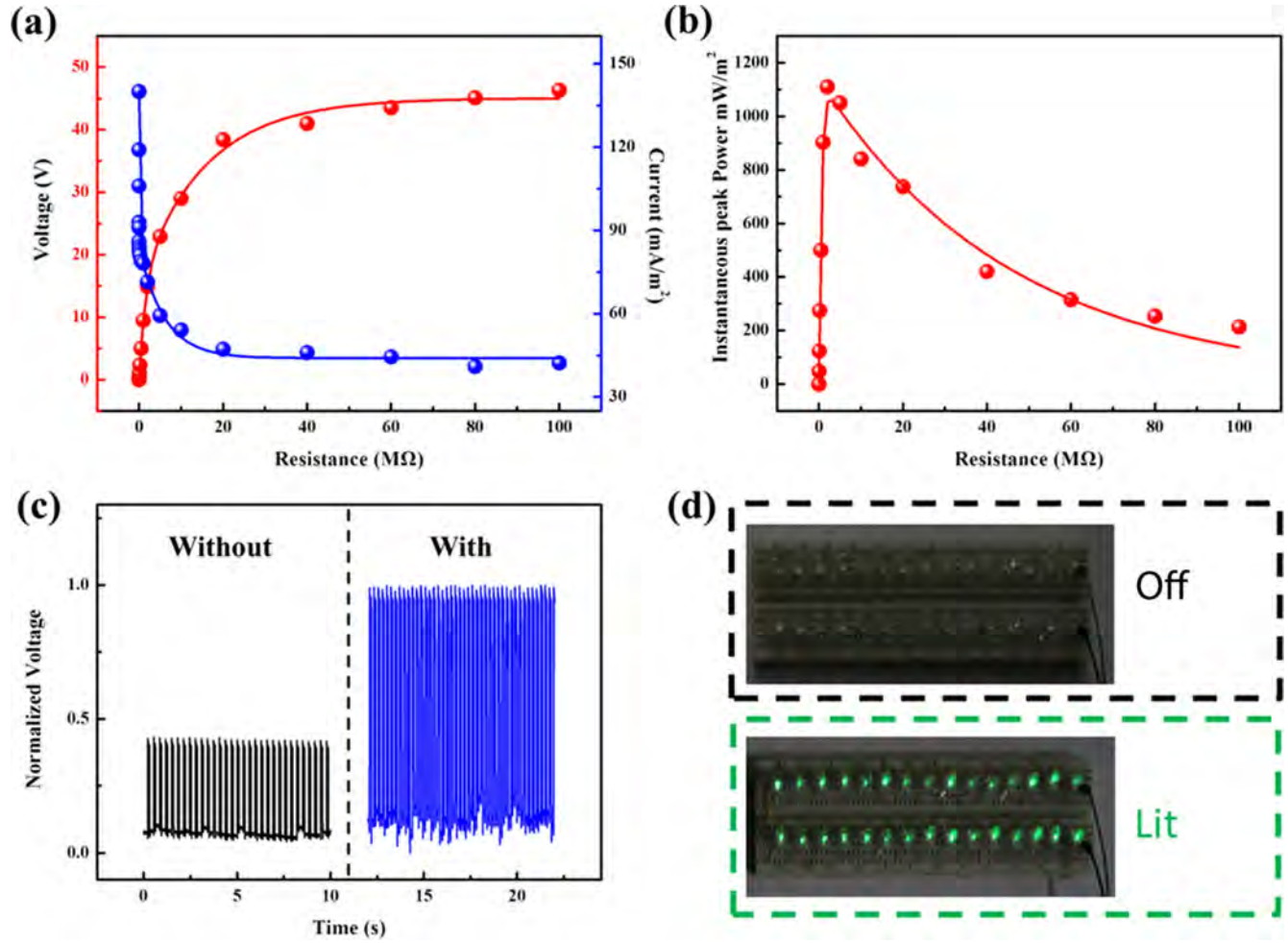

Figure 6. The typical electrical outputs of the TENG. (a) Dependence of the voltage and current density output on the external load resistance. The points represent peak value of electric signals while the lines are the fitted results. (b) Dependence of the peak power output on the resistance of the external load, indicating maximum power output when R = 2 MΩ. The curve is a fitted result. (c) The comparison of the normalized open-circuit voltage between the TENG with and without ZnOMBs. (d) A photographic image of 30commercial LED bulbs lit by the TENG at 100 Hz, without any rectifier circuit or any energy-storage elements in the whole circuit.

6.1 mA m^{-2} respectively at 1000 Hz. These two outputs are sharply increasing when the motor's frequency ranges from 0.2 Hz to 100 Hz, but grow very slowly after 100 Hz, and trend to a steady value. The typical V_{oc} and I_{sc} are elaborated in figures 5(c) and (d). Since the linear motor was performing periodic motion, the electrical outputs also presented cycle characteristics. In figure 5(d), the I_{sc} density manifested an asymmetrical-amplitude alternating behavior. Moreover, the largest and smallest peaks are generated respectively with the process of the two contact surfaces moving apart after collision and approaching each other. The phenomenon that the peak value of I_{sc} density is different in charge and discharge cycles, normally results from the I_{sc} density as a function of quantity of electricity and time, while the same number of charges are transferred back and forth when the two contact surfaces move together and apart. This phenomenon is consistent with the theoretical analysis as shown in figure 3. The glitches in signal probably result from the undulating surface of the TENG, because not all ZnOMBs are fully consistent in size.

To further investigate the output power of the TENG, resistors were provided as external loads. As displayed in figure 6(a), the instantaneous current density amplitude drops with increasing load resistance owing to the resistive loss, while the voltage follows a build-up trend. Consequently, the global maximum of the instantaneous peak power occurs when the load resistor is about 2 MΩ, corresponding to a peak power density of about 1105 mW m^{-2} (figure 6(b)), revealing that the optimal matching impedance of the TENG is 2 MΩ. Moreover, 30 commercial LED bulbs were lit at 100 Hz without any rectifier circuit or any energy-storage elements in the whole circuit, as shown in figure 6(d).

Last, to further demonstrate the effect of ZnOMBs on the electric output of the TENG, another TENG with the same structure but without any ZnOMBs was measured at the same frequency of 100 Hz. The corresponding results of the two TENGs are demonstrated in figure 6(c). From the results, the output V_{oc} of the TENG with ZnOMBs was about 2.3 times that without any ZnO, evidently revealing that the ZnOMB

surface modification can significantly improve the output efficiency of the TENG.

4. Conclusion

In summary, this work has presented an innovative enhanced TENG. The vertically aligned ZnOMBs were synthesized on the pyramid-patterned PDMS film through a low-temperature hydrothermal method. Hundreds of replicas of patterned PDMS films with vertically aligned ZnOMBs can be produced from one single mold by this method, which provides convenience for large-scale preparation. The output voltage of the fabricated TENG with ZnOMBs could reach 57 V at 100 Hz, which was about 2.3 times higher than that without any ZnO materials; moreover, the designed TENG could light 30 commercial LED bulbs without any rectifier circuits or energy-storage elements. In addition, the peak power density of the fabricated TENG could reach 1105 mW m^{-2} at an external load resistor of about 2 MΩ. All the results suggest that the incorporation of vertically aligned ZnOMBs on a pyramid-featured PDMS-based TENG can dramatically enhance the electrical output performance for various energy harvesting applications.

Acknowledgments

This work is supported by a Sichuan Province Science and Technology Plan project (No 2015JQ0013), an independent research project of the State Key Laboratory of Traction Power (No 2016TPL_Z03), the National Natural Science Foundation of China (No 51602265) and the National University Student Innovation Program (No 201510613009) of China.

References

[1] Wang Z L 2013 *ACS Nano* **7** 9533–57
[2] Hu F, Cai Q, Liao F, Shao M and Lee S T 2015 *Small* **11** 5611–28
[3] Wang Z L and Song J H 2006 *Science* **312** 242–6
[4] Wang X, Song J, Liu J and Wang Z L 2007 *Science* **316** 102–5
[5] Qin Y, Wang X and Wang Z L 2008 *Nature* **451** 809–13
[6] Wang Z L 2008 *Adv. Funct. Mater.* **18** 3553–67
[7] Wang Z L, Yang R, Zhou J, Qin Y, Xu C, Hu Y and Xu S 2010 *Mater. Sci. Eng.,* R **70** 320–9
[8] Fan F, Tian Z and Wang Z L 2012 *Nano Energy* **1** 328–34
[9] Yang W, Chen J, Zhu G, Wen X, Bai P, Su Y, Lin Y and Wang Z L 2013 *Nano Res.* **6** 880–6
[10] Wang S, Lin L and Wang Z L 2015 *Nano Energy* **11** 436–62
[11] Wang Z L, Chen J and Lin L 2015 *Energy Environ. Sci.* **8** 2250–82
[12] Zhu G, Chen J, Zhang T, Jing Q and Wang Z L 2014 *Nat. Commun.* **5** 487–507
[13] Yang J, Chen J, Liu Y, Yang W, Su Y and Wang Z L 2014 *ACS Nano* **8** 2649–57
[14] Fan X, Chen J, Yang J, Bai P, Li Z and Wang Z L 2015 *ACS Nano* **9** 4236–43
[15] Chen J *et al* 2015 *ACS Nano* **9** 3324–31
[16] Guo H, Chen J, Yeh M-H, Fan X, Wen Z, Li Z, Hu C and Wang Z L 2015 *ACS Nano* **9** 5577–84
[17] Chen J, Yang J, Guo H, Li Z, Zheng L, Su Y, Wen Z, Fan X and Wang Z L 2015 *ACS Nano* **9** 12334–43
[18] Chen J, Zhu G, Yang W, Jing Q, Bai P, Yang Y, Hou T C and Wang Z L 2013 *Adv. Mater.* **25** 6094–9
[19] Chen J, Zhu G, Yang J, Jing Q, Bai P, Yang W, Qi X, Su Y and Wang Z L 2015 *ACS Nano* **9** 105–16
[20] Yang J, Chen J, Su Y, Jing Q, Li Z, Yi F, Wen X, Wang Z and Wang Z L 2015 *Adv. Mater.* **27** 1316–26
[21] Hou T C, Yang Y, Zhang H, Chen J, Chen L J and Wang Z L 2013 *Nano Energy* **2** 856–62
[22] Zhu G, Chen J, Liu Y, Bai P, Zhou Y S, Jing Q, Pan C and Wang Z L 2013 *Nano Lett.* **13** 2282–9
[23] Yang J, Chen J, Yang Y, Zhang H, Yang W, Bai P, Su Y and Wang Z L 2014 *Adv. Energy Mater.* **4** 1301322
[24] Yang W, Chen J, Zhu G, Yang J, Bai P, Su Y, Jing Q, Cao X and Wang Z L 2013 *ACS Nano* **12** 11317–24
[25] Yang W, Chen J, Wen X, Jing Q, Yang J, Su Y, Zhu G, Wu W and Wang Z L 2014 *ACS Appl. Mater. Interfaces* **10** 7479–84
[26] Zhang L, Jin L, Zhang B, Deng W, Pan H, Tang J, Zhu M and Yang W 2015 *Nano Energy* **16** 516–23
[27] Zhang B, Chen J, Jin L, Deng W, Zhang L, Zhang H, Zhu M, Yang W and Wang Z L 2016 *ACS Nano* **10** 6241–7
[28] Zhang L, Zhang B, Chen J, Jin L, Deng W, Tang J, Zhang H, Pan H, Zhu M and Yang W 2016 *Adv. Mater.* **28** 1650–6
[29] Jin L, Chen J, Zhang B, Deng W, Zhang L, Zhang H, Huang X, Zhu M, Yang W and Wang Z L 2016 *ACS Nano* **10** 7874–81
[30] Chen J, Huang Y, Zhang N, Zou H, Liu R, Tao C, Fan X and Wang Z L 2016 *Nat. Energy* **1** 16138
[31] Wang S, Lin L and Wang Z L 2012 *Nano Lett.* **12** 6339–46
[32] Tang W, Jiang T, Fan F, Yu A, Zhang C, Cao X and Wang Z L 2015 *Adv. Funct. Mater.* **25** 3718–25
[33] Zhu G, Su Y, Bai P, Chen J, Jing Q, Yang W and Wang Z L 2014 *ACS Nano* **8** 6031–7
[34] Jing Q, Zhu G, Bai P, Xie Y, Chen J, Han R P and Wang Z L 2014 *ACS Nano* **8** 3836–42
[35] Wen X, Yang W, Jing Q and Wang Z L 2014 *ACS Nano* **8** 7405–12
[36] Bai P, Zhu G, Lin Z H, Jing Q, Chen J, Zhang G, Ma J and Wang Z L 2013 *ACS Nano* **7** 6361–6
[37] Yang W, Chen J, Jing Q, Yang J, Wen X, Su Y, Zhu G, Bai P and Wang Z L 2014 *Adv. Funct. Mater.* **24** 4090–6
[38] Jiang T, Zhang L M, Chen X, Han C B, Tang W, Zhang C, Xu L and Wang Z L 2015 *ACS Nano* **9** 12562–72
[39] Niu S, Liu Y, Chen X, Wang S, Zhou Y S, Lin L, Xie Y and Wang Z L 2015 *Nano Energy* **12** 760–74
[40] Niu S and Wang Z L 2015 *Nano Energy* **14** 161–92
[41] Zhu G, Pan C, Guo W, Chen C Y, Zhou Y, Yu R and Wang Z L 2012 *Nano Lett.* **12** 4960–5
[42] Fan F, Lin L, Zhu G, Wu W, Zhang R and Wang Z L 2012 *Nano Lett.* **12** 3109–14
[43] Hu Y, Zhang Y, Xu C, Lin L, Snyder R L and Wang Z L 2011 *Nano Lett.* **6** 2572–7
[44] Bai P, Zhu G, Zhou Y S, Wang S, Ma J, Zhang G and Wang Z L 2014 *Nano Res.* **7** 990–7
[45] Tang W, Tian J, Zheng Q, Yan L, Wang J, Li Z and Wang Z L 2015 *ACS Nano* **9** 7867–73
[46] Han M, Chen X, Yu B and Zhang H 2015 *Adv. Electron. Mater.* **1** 1500187